

## Article

# Sosnowskiy Hogweed-Based Hard Carbons for Sodium-Ion Batteries

Grigori P. Lakienko <sup>1</sup>, Zoya V. Bobyleva <sup>1,2,\*</sup>, Maria O. Apostolova <sup>1</sup>, Yana V. Sultanova <sup>1</sup>, Andrey K. Dyakonov <sup>2</sup>, Maxim V. Zakharkin <sup>2</sup>, Nikita A. Sobolev <sup>2</sup>, Anastasia M. Alekseeva <sup>2</sup>, Oleg A. Drozhzhin <sup>2,\*</sup>, Artem M. Abakumov <sup>3</sup> and Evgeny V. Antipov <sup>2,3</sup>

<sup>1</sup> Department of Material Science, Lomonosov Moscow State University, 119991 Moscow, Russia

<sup>2</sup> Department of Chemistry, Lomonosov Moscow State University, 119991 Moscow, Russia

<sup>3</sup> Skoltech Center for Energy Science and Technology, Skolkovo Institute of Science and Technology, Nobel Street 3, 143026 Moscow, Russia

\* Correspondence: zoyamostovik@gmail.com (Z.V.B.); drozhzhin@elch.chem.msu.ru (O.A.D.)

**Abstract:** Sodium-ion battery technology rapidly develops in the post-lithium-ion landscape. Among the variety of studied anode materials, hard carbons appear to be the realistic candidates because of their electrochemical performance and relative ease of production. This class of materials can be obtained from a variety of precursors, and the most ecologically important and interesting route is the synthesis from biomass. In the present work, for the first time, hard carbons were obtained from *Heracleum sosnowskiy*, a highly invasive plant, which is dangerous for humans and can cause skin burns but produces a large amount of green biomass in a short time. We proposed a simple synthesis method that includes the pretreatment stage and further carbonization at 1300 °C. The effect of the pretreatment of giant hogweed on the hard carbon electrochemical properties was studied. Obtained materials demonstrate >220 mAh g<sup>-1</sup> of the discharge capacity, high values of the initial Coulombic efficiency reaching 87% and capacity retention of 95% after 100 charge-discharge cycles in sodium half-cells. Key parameters of the materials were examined by means of different analytical, spectroscopic and microscopic techniques. The possibility of using the giant hogweed-based hard carbons in real batteries is demonstrated with full sodium-ion cells with NASICON-type Na<sub>3</sub>V<sub>2</sub>(PO<sub>4</sub>)<sub>3</sub> cathode material.

**Keywords:** biomass; hogweed; hard carbon; sodium-ion battery; anode



**Citation:** Lakienko, G.P.; Bobyleva, Z.V.; Apostolova, M.O.; Sultanova, Y.V.; Dyakonov, A.K.; Zakharkin, M.V.; Sobolev, N.A.; Alekseeva, A.M.; Drozhzhin, O.A.; Abakumov, A.M.; et al. Sosnowskiy Hogweed-Based Hard Carbons for Sodium-Ion Batteries. *Batteries* **2022**, *8*, 131.

<https://doi.org/10.3390/batteries8100131>

Academic Editors: Rui Xu, Xin Su, Zhenzhen Yang, Shitong Wang and Yutong Li

Received: 15 August 2022

Accepted: 16 September 2022

Published: 20 September 2022

**Publisher's Note:** MDPI stays neutral with regard to jurisdictional claims in published maps and institutional affiliations.



**Copyright:** © 2022 by the authors. Licensee MDPI, Basel, Switzerland. This article is an open access article distributed under the terms and conditions of the Creative Commons Attribution (CC BY) license (<https://creativecommons.org/licenses/by/4.0/>).

## 1. Introduction

Among various energy storage technologies, lithium-ion batteries (LIBs) have been widely used in portable electronics and electric vehicles. However, the galloping cost of the raw materials for LIBs is going to limit their production in the future [1,2]. Sodium is a more abundant and available element than lithium, which makes sodium ion batteries (SIBs) a promising alternative to LIBs. To bring SIB technology to the market, the electrode materials with high specific capacity and stability, as well as high Coulomb efficiency, need to be designed. However, despite the variety of cathodes for SIBs, the options for materials for the anode are quite limited. Among different carbonaceous anode materials mentioned in the literature, such as soft carbon, graphene or carbon nanotubes, a non-graphitizable carbon also known as hard carbon (HC) provides the best combination of high storage capacity and cycling stability [3]. Hard carbon could be obtained from different types of precursors, such as industrial polymer precursors, saccharides, or biomass-based precursors [4–6].

Regardless of the precursor used, hard carbon can be obtained by one-stage or two-stage synthesis. Most studies use one-step high-temperature pyrolysis as the main method for producing hard carbon from corn silk [7], waste tea [5], and argan shells [4]. In the two-stage synthesis, at the first stage, pretreatment is carried out in the form of low-temperature carbonization in air or hydrothermal carbonization, leading to the char, which is pyrolyzed at the second stage at a high temperature of 900–1600 °C. Two-stage synthesis is used for

a number of precursors, such as rape seed shuck [6], holly leaves [8] with hydrothermal carbonization as a pre-treatment, and Mango Peel [9], wheat straw and ash wood [10] with low-temperature carbonization. A pretreatment stage is one of the best strategies to increase the Coulombic efficiency and discharge capacity [11].

Among the plant biomass, it is important to find abundant, renewable, low-cost raw materials [12,13]. On the one hand, the use of selected plants should not lead to a change in ecosystem. There is also the problem of invasive plants that have become a phenomenon these days, and the consequences of which are just beginning to be noticed. For instance, such species as *Heracleum* (aka hogweed) and their distribution is of particular concern. Hogweeds are undesirable invaders, whose spread is controlled by demography, dispersal and variation in invisibility [14]. Leaves and fruits of hogweed are rich in essential oils and contain furanocoumarins [15], which leads to burns of the skin when they contact with ultraviolet radiation [16]. However, invasive hogweeds take a toll, not only on humans, but also bird communities [17], mammals, insects [18], native plants [19] and even soil [20]; therefore, the investigation and fight against hogweed is a multidisciplinary task. For the past five years, the problems of uncontrolled growth of hogweed have been actively studied [21], with technologies developed to detect hogweed for phytosanitary monitoring and its subsequent removal [22]. New implementations of hogweed have been proposed, such as extraction of coumarins and its further use as a growth stimulant [23], as well as the production of graphene nanosheets [24] from hogweed.

In this paper, we consider *Sosnowskyi* hogweed as a possible biomass-type precursor for the synthesis of hard carbon. For that purpose, we have collected dry and fresh hogweed in winter and summer, respectively. Here, we examine the influence of a pretreatment stage, namely low temperature annealing or hydrothermal carbonization, to enhance the electrochemical characteristics. Finally, the electrochemical performance of an Na-ion full cell with the NASICON-type  $\text{Na}_3\text{V}_2(\text{PO}_4)_3$  cathode is shown.

## 2. Materials and Methods

### 2.1. Materials Synthesis

#### 2.1.1. Hard Carbons (HCs)

Stems of freshly picked summer hogweed (SH) and stems of naturally dried winter hogweed (WH) were first dried at 100 °C for 24 h. Dried hogweed stems were milled, washed with water several times and then dried at 70 °C in dry air overnight.

Three routes for obtaining hard carbon samples from hogweed stems were used:

- (i) Direct pyrolysis of WH and SH in a tube furnace at 1300 °C in argon atmosphere;
- (ii) WH and SH were subjected to air pretreatment at 200 °C in the oven, which gives WH-A200 and SH-A200HCl. WH-A200 was further subjected to annealing in a tube furnace at 1300 °C in argon atmosphere. SH-A200HCl was washed with HCl, before annealing in a tube furnace at 1300 °C in argon atmosphere;
- (iii) An amount of 5 g of WH in 150 mL of deionized water was placed in the Teflon sealed autoclave (filling degree 60%) for hydrothermal pretreatment at 200 °C for 24 h, which gives WH-H200. The same procedure was used for SH but with 20 g of precursor. Intermediate products were subjected to annealing in a tube furnace at 1300 °C in argon atmosphere.

Final samples were called xH-y200-1300, where: x—S (summer) or W (winter), y—A (air pretreatment) or H (hydrothermal pretreatment), 200—temperature of pretreatment in degrees Celsius and 1300—temperature of annealing in degrees Celsius.

#### 2.1.2. $\text{Na}_3\text{V}_2(\text{PO}_4)_3$

$\text{Na}_3\text{V}_2(\text{PO}_4)_3$  (NVP) was prepared by dissolving vanadium pentoxide and citric acid in deionized water in 1:3 molar ratio, and stirring for 1 h at 70 °C. After that, the solution of 1 equivalent of sodium dihydrophosphate in deionized water was added dropwise and then the mixture was stirred at 70 °C for 1 h. Following that, the blue solution was left

at 95 °C overnight to obtain green solid residue, which was then ball-milled and finally annealed in nitrogen atmosphere at 750 °C for 8 h.

## 2.2. Materials Characterization

Thermogravimetric analysis (TGA) and differential scanning calorimetry (DSC) were carried out on an STA 449 F3 Jupiter thermal analyzer (Netzsch, Selb, Germany) over 25–500 °C range at the heating rate of 10 K/min and air flow rate of 50 mL/min.

Fourier transform infrared spectroscopy (FTIR) was performed on a Nicolet IR200 spectrometer (Thermo Fisher, Waltham, MA, USA) using KBr pellets with a resolution of 4 cm<sup>-1</sup>.

CHNSO elemental analysis was performed on a 2400 Series II CHNS/O elemental analyzer (Perkin Elmer, Waltham, MA, USA). Ash content was defined as the mass ratio of inorganic residues after annealing in air at 900 °C and dry hogweed.

Particle size and morphology were investigated using a JEOL JSM-6490LV scanning electron microscope (Tokyo, Japan).

Powder X-ray diffraction data (PXRD) were collected on a Panalytical Aeries Research diffractometer, with CuK $\alpha$  radiation ( $\lambda = 1.54182 \text{ \AA}$ ) over an angular range of 10–100° with a step size of 0.005° and exposure time of 54 s at each point (Almelo, The Netherlands). STOE WinXPOW (Version 1.2; STOE & Cie GmbH: Darmstadt, Germany, 2000) software was used for data proceeding [25].

Nitrogen adsorption/desorption isotherms measurements were performed on a NovaTouch LX2 gas sorption analyzer. All samples were preliminarily dried under vacuum at 300 °C overnight. The specific surface area was calculated by the Brunauer–Emmett–Teller (BET) method.

## 2.3. Electrode Preparation

Hard carbons were mixed with sodium carboxymethyl cellulose (CMC-Na, Ala-din) in a weight ratio of 95:5 and dissolved in deionized water. The prepared slurry was coated onto aluminum foil using a doctor blade with a thickness of 120  $\mu\text{m}$ , dried at 70 °C in the air and 15 mm disk electrodes were punched out. The electrodes were dried at 110° under dynamic vacuum. The area of electrodes was 1.8 cm<sup>2</sup> with mass loading 1–2 mg/cm<sup>2</sup> for anodes and 3 mg/cm<sup>2</sup> for cathodes.

## 2.4. Electrochemical Characterization

### 2.4.1. Half Cells

Two-electrode coin-type cells were assembled in an argon-filled glove-box (MBraun, Malsch, Germany). Sodium metal was used as a counter electrode. Galvanostatic study and cycling voltammetry were carried out using an Elins P-20X8 potentiostat-galvanostat (ES8 software) in a voltage range of 0.002–2 V vs. Na/Na<sup>+</sup> at a current density of 25 mA·g<sup>-1</sup>, followed by a constant voltage of 2 mV for 5 h. The electrolyte solution was 1M NaPF<sub>6</sub> in a mixture of 1:1 *v/v* of ethylene carbonate (EC) with diethyl carbonate (DEC) (Kishida Chemical, Osaka, Japan).

### 2.4.2. Full Cells

Before the full cells were assembled, the HC was precycled in half-cells versus sodium counter electrode to form a SEI. At the end of precycling, the Na anode was removed from the half-cell; NVP cathode was placed on an aluminum current collector, then covered with borosilicate glass separator. After that, 100  $\mu\text{L}$  of 1M NaPF<sub>6</sub> in a mixture of 1:1 *v/v* of ethylene carbonate (EC) with diethyl carbonate (DEC) (Kishida Chemical, Osaka, Japan) + 3% fluoroethylene carbonate (FEC, Sigma Aldrich, St. Louis, MI, USA) was poured as electrolyte. After that, the anode was placed over the separator. The full cell was charged galvanostatically at C/10 to 4.15 V, held for 3 h at constant voltage of 4.15 V, and discharged with 0.1 C current to 2.5 V to complete the cycle. The active mass ratio between the NVP and HC electrodes was 2.17.

### 3. Results and Discussion

#### 3.1. Pretreatment of Biomass

Three synthesis methods of HC samples from hogweed stems were carried out: direct annealing, air pretreatment followed by annealing, and hydrothermal pretreatment followed by annealing (Figure 1).

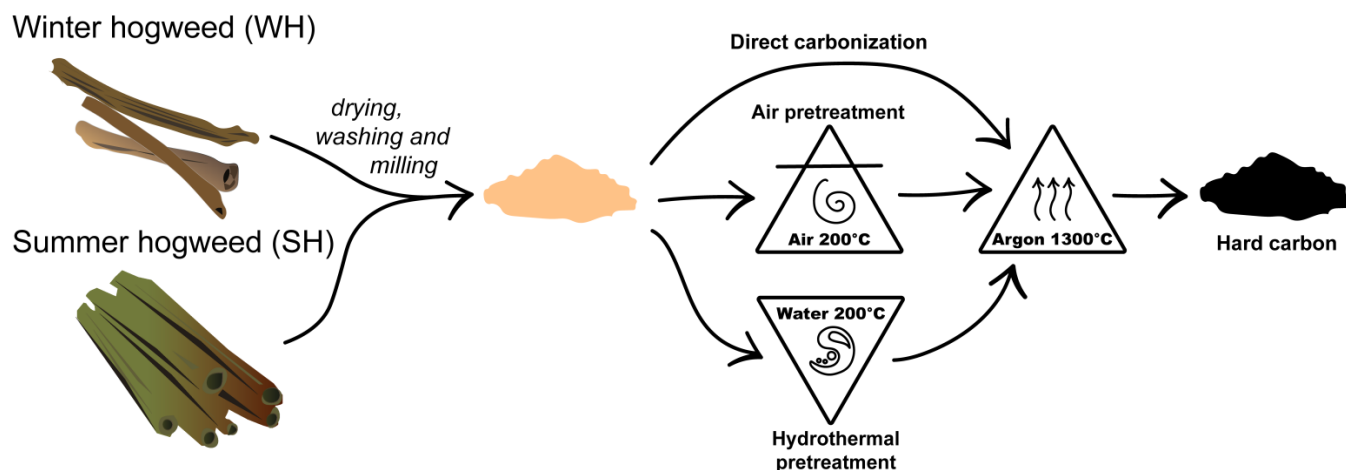


**Figure 1.** Scheme of hard carbon synthesis from hogweed.

We revealed the influence of pretreatment on the chemical composition of intermediates. For the air pretreatment, the temperature of 200 °C was chosen [26,27]. According to TG/DSC curves (Figure 2a), more intensive weight loss is observed for SH. Such a difference can be associated with higher water content in SH than that in WH. Based on TG results, the weight loss at 200 °C was 13% for SH and 5% for WH. After heat treatment at 200 °C, the color of intermediates was changed (Figure S1). Compared to the light-brown color of WH-A200, the color of SH-A200 was grayish. We assumed that the latter is associated with the presence of ash, which consists of inorganic impurities [28]. To remove them, SH-A200 was washed several times with hydrochloric acid and then with water. For further examination and the synthesis, SH-A200HCl was used.

Besides air pretreatment, hydrothermal carbonization of WH and SH at 200 °C was performed. There is no dramatic difference between the colors of the intermediates (WH-H200 and SH-H200) after hydrothermal pretreatment (Supplementary Materials, Figure S1): most probably, the majority of inorganic admixtures transfer into the solution.

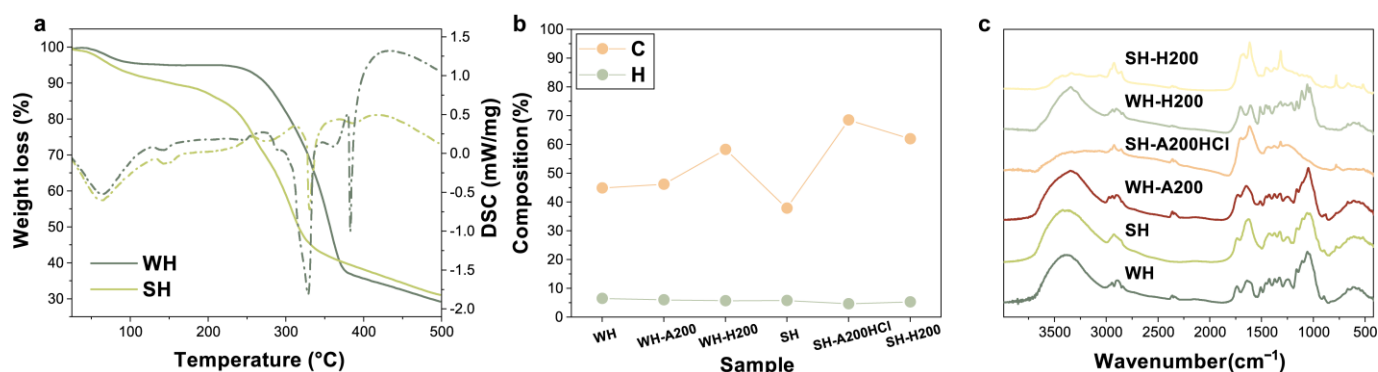


**Figure 2.** TG and DSC curves of WH and SH: (a) the results of elemental analysis (C and O in weight percent, %); (b) and FTIR spectra; (c) of winter hogweed (WH), summer hogweed (SH) and intermediate products after pretreatment.

Intermediate products after pretreatment (WH-A200, WH-H200, SH-A200HCl, and SH-H200), as well as original precursors (WH and SH), were analyzed by means of elemental

analysis (Table S1). According to the obtained results, WH and SH are slightly different in the carbon content, which is 44.8% for WH and 37.8% for SH. However, the percentage of carbon noticeably increases for SH after pretreatment. SH-A200HCl and SH-200 contain more than 60% of carbon. Air pretreatment does not have a significant effect on the carbon content in WH, which correlates well with the results of TG. However, WH after the hydrothermal pretreatment has a higher carbon content of 58.2%.

The FTIR spectra of the precursors and the intermediates are shown in Figure 2c. For all samples, the broad peak at high frequency region  $>3000\text{ cm}^{-1}$  indicates the presence of -OH functional group. The SH-A200HCl and SH-H200 have the lowest intensity of this broad peak, which is probably related to higher water loss during pretreatment. This may be due to the more open surface of the SH precursor and its better reactivity. In the low-frequency region of the FTIR spectrum there are many peaks, and most of them indicate the presence of cellulose, lignin, and hemicelluloses [29]. The peaks of C–O stretching at  $1070\text{ cm}^{-1}$  and C–H vibration at  $893\text{ cm}^{-1}$  correspond to cellulose [30,31]. The band around  $1161\text{ cm}^{-1}$  is attributed to the vibration of the C–O bond in hemicellulose [29]. The peaks at around  $1731$  and  $1642\text{ cm}^{-1}$  correspond to the C=O stretching vibration and may be attributed to aromatic groups in lignin and hemicellulose [32]. The peak at  $1600\text{ cm}^{-1}$  in SH and WH indicates the presence of C=C stretching modes, which relates to the lignin content [30]. Additionally, the peak at  $1510\text{ cm}^{-1}$  is presented in the FTIR-spectra of WH. It indicates C=C stretching modes and can occur due to a high content of lignin in WH.

For the samples after the pretreatment the peak corresponding to C=O shifts from  $1750\text{ cm}^{-1}$  to  $1670\text{ cm}^{-1}$ , probably due to increasing C=O conjugacy (the bond of ketene is  $\text{C}=\text{C}=\text{O}$ — $1648\text{ cm}^{-1}$ , the bond of ketone or aldehyde groups  $\text{C}-\text{C}=\text{O}$ — $1736\text{ cm}^{-1}$ ) [33]. This shift may prove that the intermediates also contain chars due to cross-linkage of cellulose. To sum up the results of elemental analysis and FTIR spectroscopy, the pretreatment stage affects mainly the composition of SH, and has almost no effect on WH. SH-A200HCl shows similar spectra with SH-H200 as well. Observed differences can be due to deeper conversion of SH in water solutions than in the case of WH, since the latter exhibit denser microstructure and more closed surface. We suppose that SH contains cellulose of lower molecular weight, and therefore pretreatment has a greater impact of intensity of several surface functional groups in the FTIR-spectrum.

Besides organic content, inorganic species can also be present in biomass samples. For WH, the measured ash content is 3%, and 6% is observed for SH. The composition of ash is discussed below.

### 3.2. Structure and Morphology of Giant Hogweed-Based Hard Carbons

After annealing at  $1300\text{ }^{\circ}\text{C}$  in Ar flow, the HC samples were examined by means of SEM (Figure 3). One can see that the morphology of hard carbons is inherited from the structure of hogweed stem (Figure 3a). Fibers and macropores are clearly visible, even after hydrothermal treatment (Figure 3c,f). The size of particles ranges from 10 to  $100\text{ }\mu\text{m}$  and the size distributions are non-uniform.

The type and relative amounts of inorganic impurities were studied by PXRD (Figure S2) and EDX analysis (Table S2). The main impurities found by EDX are K, Ca, Mg, Si and P, which are presented as the CaO,  $\text{CaCO}_3$ , MgO and  $\text{Ca}_5(\text{PO}_4)_3(\text{OH})$  phases in the final product (Figure S2).

Inorganic impurities in smaller quantities, especially P-containing ones, are observed in HCs after hydrothermal carbonization. We can conclude that during hydrothermal pretreatment many inorganic species were dissolved in aqueous solution [34]. The smallest amount of impurities is observed in the SH-A200HCl-1300 sample. Thus, acid pretreatment results in the purest HC materials.

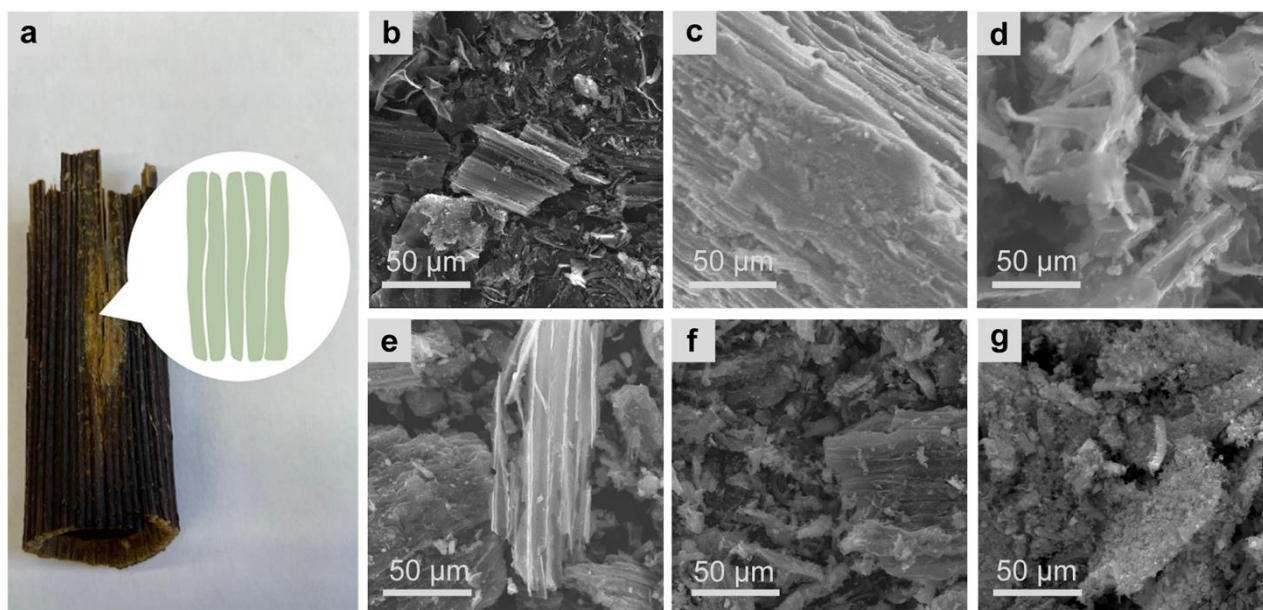


**Figure 3.** Dry stem of hogweed (a); SEM images of hard carbons SH-1300 (b); WH-A200-1300 (c); WH-H200-1300 (d); SH-1300 (e); SH-A200HCl-1300 (f); SH-H200-1300 (g).

### 3.3. Electrochemical Performance of Half and Full Cells

The obtained materials were tested in sodium half cells. Figure 4a displays the galvanostatic discharge curves for the 1st cycle at  $C/10$  ( $25 \text{ mA g}^{-1}$ ) current rate. Figure 4b and Table 1 display discharge capacity for the first cycle and initial Coulombic efficiency (ICE). It is interesting that winter samples demonstrate the largest values of the discharge capacity,  $250\sim 270 \text{ mAh g}^{-1}$ . Cycling stability of the sample with the highest capacity (Figure 4c) was also tested in a half-cell. Electrode of SH-1300 after cycling was examined by means of SEM and looked homogeneous with whole structure (Figure S3).

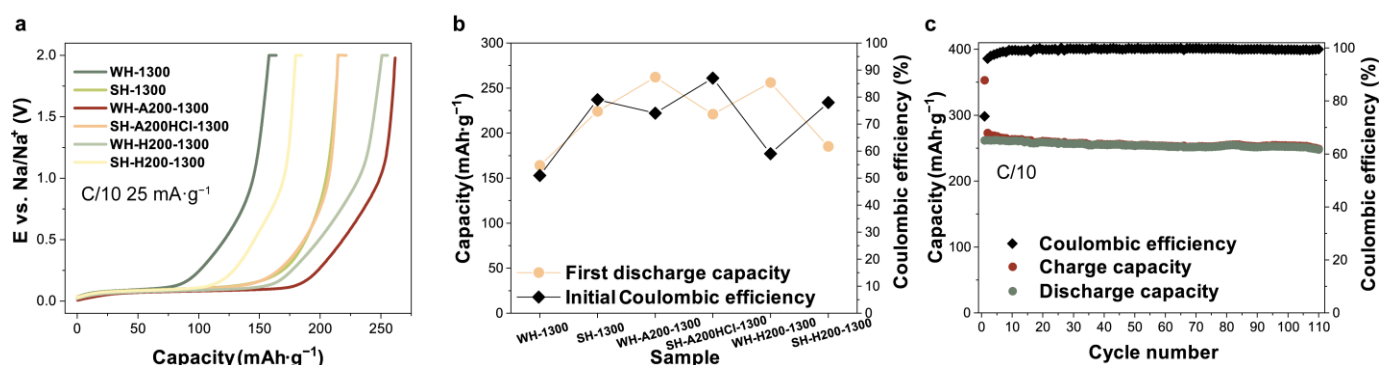


**Figure 4.** First discharge curves (a) and discharge capacity in the first cycle and initial Coulombic efficiency (b) of HC electrodes at current density of  $0.1 \text{ C}$  ( $25 \text{ mA g}^{-1}$ ); charge, discharge capacity and Coulombic efficiency for 100 cycles at  $0.1 \text{ C}$  ( $25 \text{ mA g}^{-1}$ ) of WH-A200-1300 (c).

The main findings can be summarized as follows:

(i) The SH-A200HCl-1300 sample shows the highest ICE of 87%. As mentioned above, this HC was obtained from the intermediates with the smallest quantities of inorganic impurities. Thus, the acid pretreatment can enhance the ICE of biomass-derived HCs;

(ii) BET surface area measurements correlate with the ICE of the obtained HCs (Table 1). For example, the lowest ICE of 51% is observed for WH-1300 with the highest surface area of  $337 \text{ m}^2 \text{ g}^{-1}$ . SH-A200HCl-1300 demonstrated the lowest BET surface area and the highest ICE. The correlation between surface area and ICE arises primarily from the electrolyte decomposition and formation of SEI. The intensity of this process is in a quite

direct dependence on the surface area [3,35]. The acid pretreatment can contribute to the removal of inorganic impurities that cause self-activation at high temperatures and create pore structures, and can therefore lead to a significant surface area reduction [36];

(iii) Discharge capacities of the WH samples after pretreatment are higher than SH ones after pretreatment, although their ICE is lower;

(iv) The pretreatment stage can help to improve electrochemical performance in case of winter hogweed samples;

(v) WH-A200-1300 shows the highest discharge capacity and good capacity retention after 100 cycles of 95% at a current density of C/10 ( $25 \text{ mA g}^{-1}$ ).

**Table 1.** Discharge specific capacity, Coulombic efficiency of the first cycle and BET specific surface area of HCs.

Sample	Discharge Specific Capacity, $\text{mAh g}^{-1}$	Coulombic Efficiency (%)	$S_{\text{BET}}$ ( $\text{m}^2 \text{g}^{-1}$ )
WH-1300	164	51	337
SH-1300	224	79	57
WH-A200-1300	262	74	29
SH-A200HCl-1300	221	87	7
WH-H200-1300	256	59	127
SH-H200-1300	185	78	27

Additionally, the WH-A200-1300 sample was tested in a full cell versus the  $\text{Na}_3\text{V}_2(\text{PO}_4)_3$  cathode material. Figure 5 displays galvanostatic charge–discharge curves of the cell at C/10 ( $11.7 \text{ mA g}^{-1}$ ). It shows good reversible discharge capacity of  $106 \text{ mAh g}^{-1}$  (normalized to the cathode mass) and capacity retention of 76% after 75 cycles.

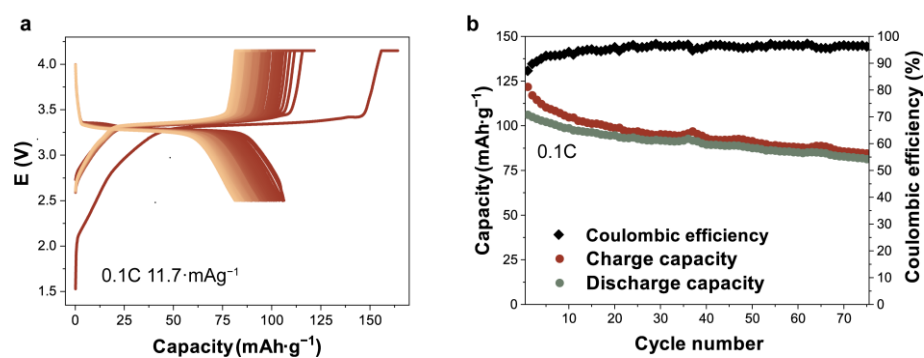


**Figure 5.** Charge–discharge curves (a) and charge–discharge capacity and Coulombic efficiency during cycling (b) of full cell at current density C/10 ( $11.7 \text{ mA g}^{-1}$ ).

To summarize the results, we have shown that several factors are supposed to influence the composition, microstructure and, respectively, electrochemical performance of hogweed-derived HC. First, the origin of the precursor plays the great role. In this paper, we used stems of giant hogweed, which were collected in winter (WH) and in summer (SH). SH contains a large amount of water and needs additional drying. Apparently, complex drying can help to improve electrochemical performance of samples produced from SH. To consider the environmental problem of hogweed dissemination, it is preferable and useful to pick up the fresh stems of hogweed. However, the last one is more dangerous for people because it contains toxic organic compounds (e.g., furanocoumarins), which are not presented in dry winter hogweed [37]. Second, the pretreatment step is crucial for improving the ICE. According to many works [38], HCl washing can modify the carbonaceous matrix in the intermediates and can almost completely remove the inorganic impurities. Finally,

to the best of our knowledge, the presented HCs demonstrate one of the best results for biomass-derived HC from the point of view of its electrochemical performance (Table S3).

#### 4. Conclusions

Sosnowski hogweed proved to be a good organic precursor for plant-derived hard carbon anode materials for SIBs. Different methods of treatment allow tuning the material's composition, microstructure and electrochemical performance. The HCs obtained from fresh stems of hogweed, which have been collected in summer, show better ICE, although naturally dried winter samples demonstrate higher discharge capacity. HCl pretreatment of the intermediate product results in reduced amounts of inorganic impurities and surface area, which help to increase the ICE up to 87%. The hogweed-derived HCs demonstrate stable cycling performance in sodium half-cells and full cells with NVP cathode material.

**Supplementary Materials:** The following supporting information can be downloaded at: <https://www.mdpi.com/article/10.3390/batteries8100131/s1>, Figure S1: Photo images of winter (WH) (a) and summer (SH) (d) hogweed stems and intermediate products WH-A200 (b), WH-H200 (c), SH-A200HCl before HCl treatment (e), SH-H200 (f); Table S1: Results of CHNSO analysis. Results presented as weight percent  $\pm$  standard deviation ( $n = 3$ ); Figure S2: PXRD data of different hard carbons; Table S2: Results of the EDX analysis of HC samples; Figure S3: SEM images of SH-1300 electrode after 10 cycles at C/10; Table S3: Comparison with hard carbon from the literature. References [39–43] are cited in the supplementary materials.

**Author Contributions:** Conceptualization, Z.V.B. and G.P.L.; methodology, G.P.L. and Z.V.B.; investigation, Z.V.B., G.P.L., Y.V.S. and A.K.D.; formal analysis, N.A.S. and A.M.A. (Anastasia M. Alekseeva); writing—original draft preparation, G.P.L., M.O.A., Z.V.B. and A.K.D.; writing—review and editing, M.V.Z., O.A.D., A.M.A. (Artem M. Abakumov) and E.V.A.; supervision, O.A.D. and E.V.A.; project administration, E.V.A.; funding acquisition, E.V.A. All authors have read and agreed to the published version of the manuscript.

**Funding:** This work was supported by the Russian Science Foundation (grant No. 17-73-30006).

**Institutional Review Board Statement:** Not applicable.

**Informed Consent Statement:** Not applicable.

**Data Availability Statement:** Not applicable.

**Acknowledgments:** Authors are grateful to I. Kalinin for providing winter hogweed (WH) samples and O. Sultanova with M. Bochkov for summer hogweed (SH) samples. Authors would also like to thank A. Kubarkov and Y. Golubev for providing the TGA/DSC data. Elemental analysis was carried out using the equipment of the MSU Shared Research Equipment Center “Technologies for obtaining new nanostructured materials and their complex study” and purchased by MSU in the frame of the Equipment Renovation Program (National Project “Science”).

**Conflicts of Interest:** The authors declare no conflict of interest.

#### References

1. Tarascon, J.M. Is Lithium the New Gold? *Nat. Chem.* **2010**, *2*, 510. [[CrossRef](#)] [[PubMed](#)]
2. Martin, G.; Rentsch, L.; Höck, M.; Bertau, M. Lithium Market Research—Global Supply, Future Demand and Price Development. *Energy Storage Mater.* **2017**, *6*, 171–179. [[CrossRef](#)]
3. Saurel, D.; Orayech, B.; Xiao, B.; Carriazo, D.; Li, X.; Rojo, T. From Charge Storage Mechanism to Performance: A Roadmap toward High Specific Energy Sodium-Ion Batteries through Carbon Anode Optimization. *Adv. Energy Mater.* **2018**, *8*, 1703268. [[CrossRef](#)]
4. Dahbi, M.; Kiso, M.; Kubota, K.; Horiba, T.; Chafik, T.; Hida, K.; Matsuyama, T.; Komaba, S. Synthesis of Hard Carbon from Argan Shells for Na-Ion Batteries. *J. Mater. Chem. A Mater.* **2017**, *5*, 9917–9928. [[CrossRef](#)]
5. Pei, L.; Cao, H.; Yang, L.; Liu, P.; Zhao, M.; Xu, B.; Guo, J. Hard Carbon Derived from Waste Tea Biomass as High-Performance Anode Material for Sodium-Ion Batteries. *Ionics* **2020**, *26*, 5535–5542. [[CrossRef](#)]
6. Cao, L.; Hui, W.; Xu, Z.; Huang, J.; Zheng, P.; Li, J.; Sun, Q. Rape Seed Shuck Derived-Lamellar Hard Carbon as Anodes for Sodium-Ion Batteries. *J. Alloy. Compd.* **2017**, *695*, 632–637. [[CrossRef](#)]

7. Nita, C.; Zhang, B.; Dentzer, J.; Matei Ghimbeu, C. Hard Carbon Derived from Coconut Shells, Walnut Shells, and Corn Silk Biomass Waste Exhibiting High Capacity for Na-Ion Batteries. *J. Energy Chem.* **2021**, *58*, 207–218. [[CrossRef](#)]
8. Zheng, P.; Liu, T.; Yuan, X.; Zhang, L.; Liu, Y.; Huang, J.; Guo, S. Enhanced Performance by Enlarged Nano-Pores of Holly Leaf-Derived Lamellar Carbon for Sodium-Ion Battery Anode. *Sci. Rep.* **2016**, *6*, 26246. [[CrossRef](#)]
9. Muruganantham, R.; Wang, F.M.; Yuwono, R.A.; Sabugaa, M.; Liu, W.R. Biomass Feedstock of Waste Mango-Peel-Derived Porous Hard Carbon for Sustainable High-Performance Lithium-Ion Energy Storage Devices. *Energy Fuels* **2021**, *35*, 10878–10889. [[CrossRef](#)]
10. Saavedra Rios, C.d.M.; Simone, V.; Simonin, L.; Martinet, S.; Dupont, C. Biochars from Various Biomass Types as Precursors for Hard Carbon Anodes in Sodium-Ion Batteries. *Biomass Bioenergy* **2018**, *117*, 32–37. [[CrossRef](#)]
11. Xu, Z.; Wang, J.; Guo, Z.; Xie, F.; Liu, H.; Yadegari, H.; Tebyetekerwa, M.; Ryan, M.P.; Hu, Y.S.; Titirici, M.M. The Role of Hydrothermal Carbonization in Sustainable Sodium-Ion Battery Anodes. *Adv. Energy Mater.* **2022**, *12*, 2200208. [[CrossRef](#)]
12. Cheng, Y.; Ji, S.; Xu, X.; Liu, J. Wheat Straw Carbon Matrix Wrapped Sulfur Composites as a Superior Cathode for Li–S Batteries. *RSC Adv.* **2015**, *5*, 100089–100096. [[CrossRef](#)]
13. Liu, J.; Kopold, P.; van Aken, P.A.; Maier, J.; Yu, Y. Energy Storage Materials from Nature through Nanotechnology: A Sustainable Route from Reed Plants to a Silicon Anode for Lithium-Ion Batteries. *Angew. Chem.* **2015**, *127*, 9768–9772. [[CrossRef](#)]
14. Koldasbayeva, D.; Tregubova, P.; Shadrin, D.; Gasanov, M.; Pukalchik, M. Large-Scale Forecasting of Heracleum Sosnowskyi Habitat Suitability under the Climate Change on Publicly Available Data. *Sci. Rep.* **2022**, *12*, 6128. [[CrossRef](#)] [[PubMed](#)]
15. Kulikov, O.A.; Ageev, V.P.; Brodovskaya, E.P.; Shlyapkina, V.I.; Petrov, P.S.; Zharkov, M.N.; Yakobson, D.E.; Maev, I.V.; Sukhorukov, G.B.; Pyataev, N.A. Evaluation of Photocytotoxicity Liposomal Form of Furanocoumarins Sosnowsky’s Hogweed. *Chem. Biol. Interact.* **2022**, *357*, 109880. [[CrossRef](#)] [[PubMed](#)]
16. Baker, B.G.; Bedford, J.; Kanitkar, S. Keeping Pace with the Media; Giant Hogweed Burns—A Case Series and Comprehensive Review. *Burns* **2017**, *43*, 933–938. [[CrossRef](#)]
17. Grzędzicka, E. Impact of Invasive Weeds on the Diversity and Dissimilarity of Bird Communities in Forested Areas. *Diversity* **2022**, *14*, 229. [[CrossRef](#)]
18. Ustinova, E.N.; Savina, K.A.; Lysenkov, S.N. New Data on Consortive Associations of Sosnowsky’s Hogweed with Anthophilous Insects. *Russ. J. Biol. Invasions* **2017**, *8*, 375–385. [[CrossRef](#)]
19. Thiele, J. Patterns and Processes of Heracleum Mantegazzianum Invasion into German Cultural Landscapes on the Local, Landscape and Regional Scale. Ph.D. Thesis, Justus-Liebig University Gießen, Gießen, Germany, 2007.
20. Renčo, M.; Jurová, J.; Gömöryová, E.; Čerevková, A. Long-Term Giant Hogweed Invasion Contributes to the Structural Changes of Soil Nematofauna. *Plants* **2021**, *10*, 2103. [[CrossRef](#)]
21. Menshchikov, A.; Shadrin, D.; Prutyaynov, V.; Lopatkin, D.; Sosnin, S.; Tsykunov, E.; Iakovlev, E.; Somov, A. Real-Time Detection of Hogweed: UAV Platform Empowered by Deep Learning. *IEEE Trans. Comput.* **2021**, *70*, 1175–1188. [[CrossRef](#)]
22. Kornilov, T.; Terentev, A.; Kekelidze, V. Use of a Hardware-Software Complex for Phytosanitary Monitoring and Chemical Treatments of the Sosnowski Hogweed. *BIO Web. Conf.* **2020**, *18*, 00015. [[CrossRef](#)]
23. Andreeva, L.v. Sosnowsky Hogweed: New Ways to Use. *IOP Conf. Ser. Earth Environ. Sci.* **2020**, *613*, 012006. [[CrossRef](#)]
24. Voznyakovskii, A.P.; Neverovskaya, A.Y.; Voznyakovskii, A.A.; Karmanov, A.P.; Shugalei, I.V. Hogweed Biomass as a Raw Material for Producing 2D Nanocarbons: An Environmental Aspect. *Russ. J. Gen. Chem.* **2020**, *90*, 2627–2631. [[CrossRef](#)]
25. S. WinXPOW. Version 1.2; STO E & Cie GmbH: Darmstadt, Germany, 2000.
26. Lin, X.; Liu, Y.; Tan, H.; Zhang, B. Advanced Lignin-Derived Hard Carbon for Na-Ion Batteries and a Comparison with Li and K Ion Storage. *Carbon* **2020**, *157*, 316–323. [[CrossRef](#)]
27. Du, Y.F.; Sun, G.H.; Li, Y.; Cheng, J.Y.; Chen, J.P.; Song, G.; Kong, Q.Q.; Xie, L.J.; Chen, C.M. Pre-Oxidation of Lignin Precursors for Hard Carbon Anode with Boosted Lithium-Ion Storage Capacity. *Carbon* **2021**, *178*, 243–255. [[CrossRef](#)]
28. del Mar Saavedra Rios, C.; Simonin, L.; Ghimbeu, C.M.; Vaulot, C.; da Silva Perez, D.; Dupont, C. Impact of the Biomass Precursor Composition in the Hard Carbon Properties and Performance for Application in a Na-Ion Battery. *Fuel Process. Technol.* **2022**, *231*, 107223. [[CrossRef](#)]
29. Satbaev, B.; Yefremova, S.; Zharmenov, A.; Kablanbekov, A.; Yermishin, S.; Shalabaev, N.; Satbaev, A.; Khen, V. Rice Husk Research: From Environmental Pollutant to a Promising Source of Organo-Mineral Raw Materials. *Materials* **2021**, *14*, 4119. [[CrossRef](#)]
30. De Oliveira, J.P.; Bruni, G.P.; Lima, K.O.; el Halal, S.L.M.; da Rosa, G.S.; Dias, A.R.G.; Zavareze, E.D.R. Cellulose Fibers Extracted from Rice and Oat Husks and Their Application in Hydrogel. *Food Chem.* **2017**, *221*, 153–160. [[CrossRef](#)]
31. Johar, N.; Ahmad, I.; Dufresne, A. Extraction, Preparation and Characterization of Cellulose Fibres and Nanocrystals from Rice Husk. *Ind. Crop. Prod.* **2012**, *37*, 93–99. [[CrossRef](#)]
32. Daffalla, S.B.; Mukhtar, H.; Shaharun, M.S. Characterization of Adsorbent Developed from Rice Husk: Effect of Surface Functional Group on Phenol Adsorption. *J. Appl. Sci.* **2010**, *10*, 1060–1067. [[CrossRef](#)]
33. Abdelkafi, F.; Ammar, H.; Rousseau, B.; Tessier, M.; el Gharbi, R.; Fradet, A. Structural Analysis of Alfa Grass (*Stipa tenacissima* L.) Lignin Obtained by Acetic Acid/Formic Acid Delignification. *Biomacromolecules* **2011**, *12*, 3895–3902. [[CrossRef](#)] [[PubMed](#)]
34. Wang, J.; Yan, L.; Ren, Q.; Fan, L.; Zhang, F.; Shi, Z. Facile Hydrothermal Treatment Route of Reed Straw-Derived Hard Carbon for High Performance Sodium Ion Battery. *Electrochim. Acta* **2018**, *291*, 188–196. [[CrossRef](#)]
35. Kumar, H.; Detsi, E.; Abraham, D.P.; Shenoy, V.B. Fundamental Mechanisms of Solvent Decomposition Involved in Solid-Electrolyte Interphase Formation in Sodium Ion Batteries. *Chem. Mater.* **2016**, *28*, 8930–8941. [[CrossRef](#)]

36. Wang, J.; Zhao, J.; He, X.; Qiao, Y.; Li, L.; Chou, S.-L. Hard Carbon Derived from Hazelnut Shell with Facile HCl Treatment as High-Initial-Coulombic-Efficiency Anode for Sodium Ion Batteries. *Sustain. Mater. Technol.* **2022**, *33*, e00446. [[CrossRef](#)]
37. Mishyna, M.; Laman, N.; Prokhorov, V.; Fujii, Y. Angelicin as the Principal Allelochemical in *Heracleum sosnowskyi* Fruit. *Nat. Prod. Commun.* **2015**, *10*, 767–770. [[CrossRef](#)]
38. Susanti, R.F.; Alvin, S.; Kim, J. Toward High-Performance Hard Carbon as an Anode for Sodium-Ion Batteries: Demineralization of Biomass as a Critical Step. *J. Ind. Eng. Chem.* **2020**, *91*, 317–329. [[CrossRef](#)]
39. Liu, H.; Liu, X.; Wang, H.; Zheng, Y.; Zhang, H.; Shi, J.; Liu, W.; Huang, M.; Kan, J.; Zhao, X.; et al. High-Performance Sodium-Ion Capacitor Constructed by Well-Matched Dual-Carbon Electrodes from a Single Biomass. *ACS Sustain. Chem. Eng.* **2019**, *14*, 12188–12199. [[CrossRef](#)]
40. Ren, X.; Xu, S.D.; Liu, S.; Chen, L.; Zhang, D.; Qiu, L. Lath-Shaped Biomass Derived Hard Carbon as Anode Materials with Super Rate Capability for Sodium-Ion Batteries. *J. Electroanal. Chem.* **2019**, *841*, 63–72. [[CrossRef](#)]
41. Arie, A.A.; Tekin, B.; Demir, E.; Demir-Cakan, R. Utilization of The Indonesian's Spent Tea Leaves as Promising Porous Hard Carbon Precursors for Anode Materials in Sodium Ion Batteries. *Waste Biomass Valor.* **2020**, *6*, 3121–3131. [[CrossRef](#)]
42. Gaddam, R.R.; Jiang, E.; Amiralian, N.; Annamalai, P.K.; Martin, D.J.; Kumar, N.A.; Zhao, X.S. Spinifex Nanocellulose Derived Hard Carbon Anodes for High-Performance Sodium-Ion Batteries. *Sustain. Energy Fuels* **2017**, *5*, 1090–1097. [[CrossRef](#)]
43. Li, Y.; Lu, Y.; Meng, Q.; Jensen, A.C.S.; Zhang, Q.; Zhang, Q.; Tong, Y.; Qi, Y.; Gu, L.; Titirici, M.-M.; et al. Regulating Pore Structure of Hierarchical Porous Waste Cork-Derived Hard Carbon Anode for Enhanced Na Storage Performance. *Adv. Energy Mater.* **2019**, *48*, 1902852. [[CrossRef](#)]